43rd AIAA Aerospace Sciences Meeting and Exhibit, Jan 10–13, Reno, Nevada

Numerical Analysis of the Bleed Slot Design of the Purdue Mach 6 Wind Tunnel

Ezgi S. Taskinoglu* and Doyle D. Knight†
Dept of Mechanical and Aerospace Eng,
Rutgers - The State University of New Jersey,
98 Brett Road, Piscataway, NJ 08854-8058

Steven P. Schneider‡
School of Aeronautics and Astronautics,
Purdue University,
West Lafayette, IN 47907-1282

One of the major challenges in hypersonic flow research is the accurate prediction of transition location. There is a wide range of scatter in transition data obtained from numerous experiments conducted since the 1960's. It is believed that most of the experimental data obtained in conventional ground test facilities are contaminated by high levels of noise due to acoustic fluctuations from the turbulent boundary layers on the wind tunnel walls. One method to reduce noise is to delay boundary layer transition using, among other features, bleed slots before the nozzle throat. The Purdue Mach 6 quiet tunnel has been designed to reduce the noise level an order of magnitude below that in conventional facilities. However, in this tunnel quiet flow is achieved only for low Reynolds numbers. For high Reynolds numbers the level of noise measured in the test section is dominated by early transition of the boundary layer on the tunnel walls which now appears to be caused by laminar boundary layer separation at the bleed slot. This paper summarizes the numerical analysis performed for one of the bleed slot designs of the Purdue Mach 6 quiet tunnel. The objective of the numerical study is to understand the effect of bleed slot design on the wind tunnel performance where the slot is considered as an upstream perturbation source. The steady state numerical solutions for two different stagnation pressures are obtained and analyzed using a commercial flow solver GASPex, version 4.1.0+. To quantify the numerical error in the solutions, a grid sensitivity analysis is conducted. For comparison purposes the Langley Mach 6 quiet tunnel is also analyzed numerically. The presence of large separation on the bleed lip of the unsuccessful Purdue tunnel, and the absence of large separation on the successful Langley tunnel, suggests that the separations are the most likely cause of early transition in the Purdue facility.

Nomenclature

γ	Ratio of specific heats
ρ	Density
a	Speed of sound
M	Mach number
P	Pressure
R	Universal gas constant

*Postdoctoral Associate, Dept of Mechanical and Aerospace Engineering; Member, AIAA.
†Professor, Dept of Mechanical and Aerospace Engineering; Associate Fellow, AIAA.
‡Professor, School of Aeronautics and Astronautics; Associate Fellow, AIAA.

R^- Riemann invariant for right running characteristics
T Temperature
u, v, w Velocity components in x, y, z directions, respectively

Subscripts

b Boundary cell values
c First interior cell values
o Stagnation values

I. Introduction

THERE are large differences in heat transfer rates, skin friction drag, stability and control effectiveness between laminar and turbulent boundary layers in hypersonic flow. It is important, therefore, to have reliable capabilities in predicting boundary layer transition to optimize hypersonic vehicle performance.[1] The noise radiated from the turbulent boundary layers on wind tunnel walls, however, contaminates the wind tunnel measurements. Thus, conventional wind tunnels having much higher disturbance levels compared to actual flight conditions are not reliable for predicting hypersonic boundary layer transition in flight.[2] The Purdue Mach 6 quiet tunnel has been designed to reduce the noise level an order of magnitude below that in conventional facilities. It is built as a Ludwieg tube which is a long pipe having a converging-diverging nozzle on the end followed by a test section. An expansion wave travels upstream through the test section when the diaphragm located downstream of the test section bursts. Expansion-wave reflections take place for a period of time during which the flow remains quiet and the pressure drops quasi-statically. For noise reduction, modifications such as the use of a highly polished nozzle and the installations of bleed slots for the contraction wall boundary layer are made. However, the tunnel, which has been operational since 2001, is not yet quiet for Reynolds numbers higher than 2×10^5. One of the possible causes for the lack of quiet flow is thought to be fluctuations generated at the nozzle throat due to flawed bleed slot design.[3] Thus, the original design of the bleed slot has been modified and altogether seven different bleed slot designs have been built and tested.[3,4,5] The bleed slot cases 1 to 5 did not yield any quiet flow.[3] The bleed slot case 6 provided quiet flow for low Reynolds numbers of about 2×10^5.[4] The bleed slot case 7 was built as an attempt to achieve quiet flow at higher Reynolds numbers; however, it gave a similar performance to bleed slot case 6, *i.e.*, quiet flow for stagnation pressures below 8 psia.[5]

The bleed slot design of the R1Ch Mach-3 quiet tunnel at ONERA, France has been numerically analyzed to investigate the flow physics for different bleed slot mass flow rates and locations.[6,7] Their analysis shows that a flawed bleed slot design can cause separation bubbles in the nozzle wall leading to early transition of the boundary layers on the tunnel walls. Based on the bleed slot mass flow rate, three different bleed slot geometries are studied, namely, adapted, weak and strong suction (Fig. 1). For strong suction, a stagnation point is observed on the inner surface of the bleed slot lip, creating a recirculation region on the outer wall. For weak suction, however, the stagnation point moves to the outer surface of the lip, leading to recirculation region on the inner wall. Both of these configurations can cause perturbations to the downstream flow. The latter design may be particularly harmful because it creates noise directly in the downstream flow increasing the risk of early transition of the boundary layer on the tunnel walls. The case of strong suction could also cause perturbations in the main flow, if the mass flow through the slot becomes unsteady, causing unsteady oscillations on the stagnation point on the bleed lip. The adapted suction is the optimal design with which no separation due to bleed slot installation is observed.[6]

In this paper, a numerical analysis for the bleed slot design case 7 of the Purdue Mach-6 quiet tunnel is presented. Numerical solutions for two different stagnation pressures are analyzed to investigate the effects of different stagnation pressures on the flow behavior near the bleed slot lip. The steady state numerical solutions are obtained using a commercial flow solver GASPex, version 4.1.0+.[8] A grid sensitivity analysis is conducted to quantify the numerical error in the solutions. In addition, the Langley Mach 6 quiet tunnel is numerically analyzed for comparison purposes.

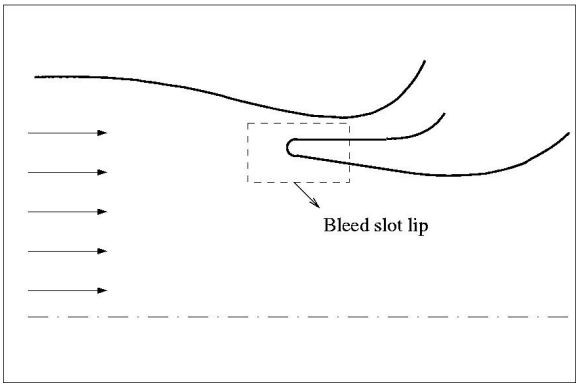

(a) Bleed slot lip

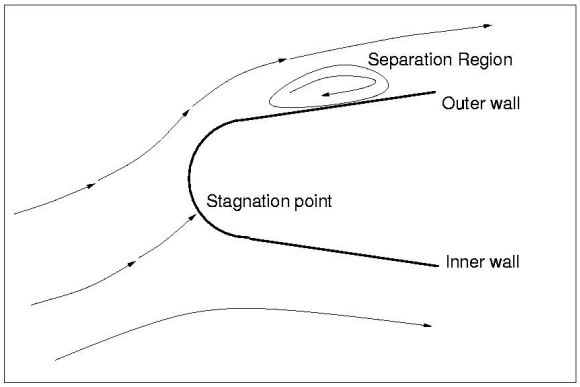

(b) Strong suction

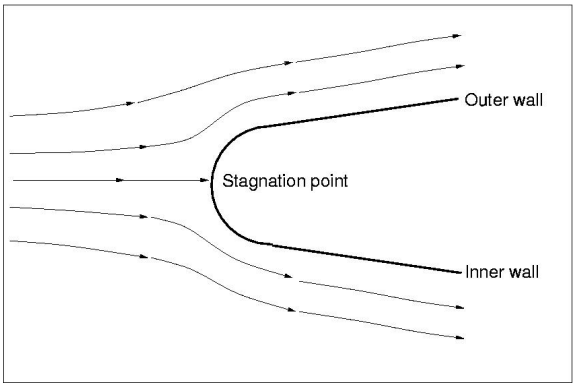

(c) Adapted suction

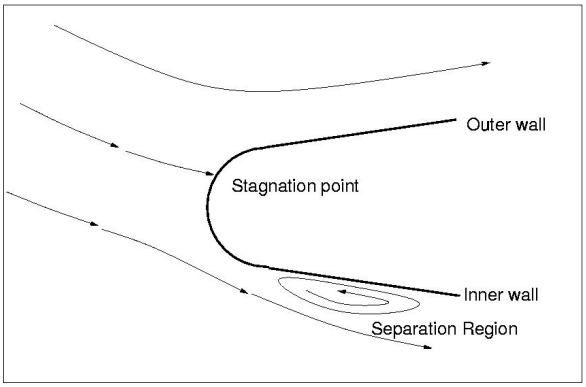

(d) Weak suction

Figure 1. Schematic representation

II. Problem Description

A. Geometry

The axisymmetric flow domain for both the Purdue and Langley tunnels is represented mainly by two surface contours (Fig. 2). For the Purdue tunnel, the contraction surface that starts from $x = -1034$ mm is the first contour. The second contour is the nozzle surface that includes the bleed slot geometry and ends at $x = 120$ mm. Both surfaces are created using the data provided by Prof. Schneider for bleed slot design case 7.[5] The origin of the coordinates is chosen to be the nozzle throat. The hemisphere at the slot tip has a diameter of 0.762 mm. The radial and axial location of the hemisphere center are $-24.646, 18.067$ mm, respectively. The hemisphere is represented by more than 100 data points. The nozzle throat radius is 15.69 mm. Similarly, the Langley tunnel geometry is defined by two surfaces, a contraction surface starting from -500 mm and a nozzle surface ending at 68 mm (Fig. 2b). The hemisphere at the bleed slot tip has a diameter of 0.254 mm. This value is three times smaller than the hemisphere diameter of Purdue tunnel bleed slot. The outer wall of the bleed slot for the Langley tunnel is positioned with an angle to the axis of symmetry which provides a smooth outlet. Flow that leaves the Purdue tunnel bleed slot, however, experiences a 90^o turn. In addition, the contraction surface of the Langley tunnel has a larger slope.

B. Grid Generation

GridPro,[9] developed by Program Development Corporation, is utilized for mesh generation. The grid block topology with eight zones is displayed in Fig. 3a. The close-up view near the slot can also be seen in this figure. The number of points for each zone is tabulated in Table 1. Grid clustering is performed using the first cell height of 10^{-5}m and stretching parameter of 1.105. The total number of grid points is $38,984$. For the Langley tunnel a grid block topology of nine zones is used (Fig. 3b). The first cell height is lowered to 10^{-6}m and a finer grid resolution is created. The number of points used for each zone is tabulated in Table 2. The total number of grid points is $116,432$. The generated grid for both tunnels are shown in Fig. 4. It is critical to have enough number of grid points around the bleed slot lip to keep a smooth representation of the geometry. Since the bleed slot lip has a very small diameter compared to the rest of the geometry, grid sizes vary throughout the computational domain.

Table 1. Number of grid points used in each zone for Grid No.1 - Purdue Tunnel

Zone	1	2	3	4	5	6	7	8
Grid	461×27	5×209	28×369	41×269	5×153	25×137	9×17	25×65
							Total	$= 38,984$

Table 2. Number of grid points used in each zone for Grid No.1 - the Langley Tunnel

Zone	1	2	3	4	5	6	7	8	9
Grid	66×593	41×321	417×43	353×9	115×289	17×17	113×33	129×49	257×9
								Total	$= 116,432$

C. Run Definitions

There are three run definitions. The first and the second are for the Purdue tunnel computations. They differ only in specified inflow stagnation pressure. The last run definition is for the Langley tunnel computation.

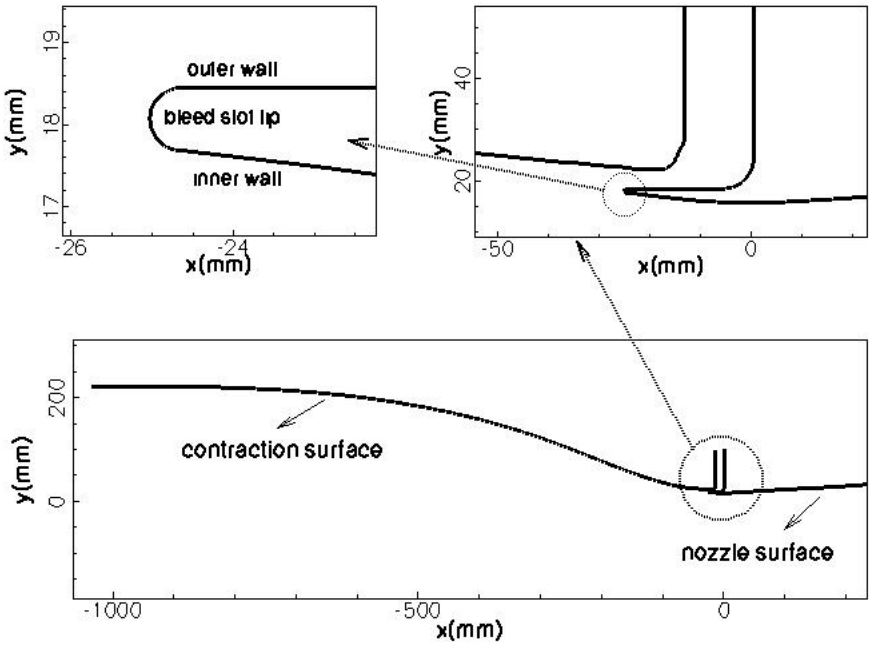

(a) Purdue Tunnel

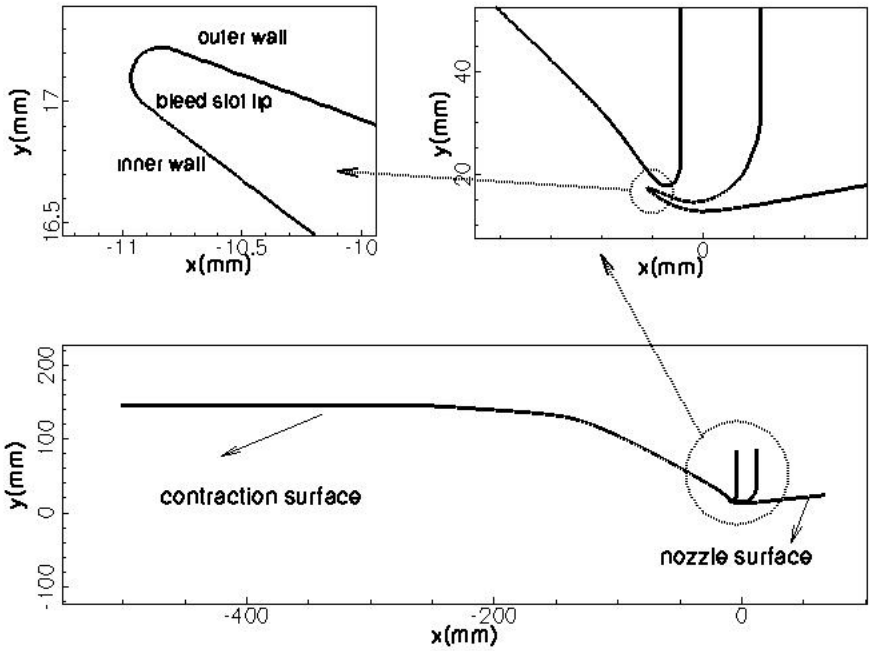

(b) Langley Tunnel

Figure 2. Geometry

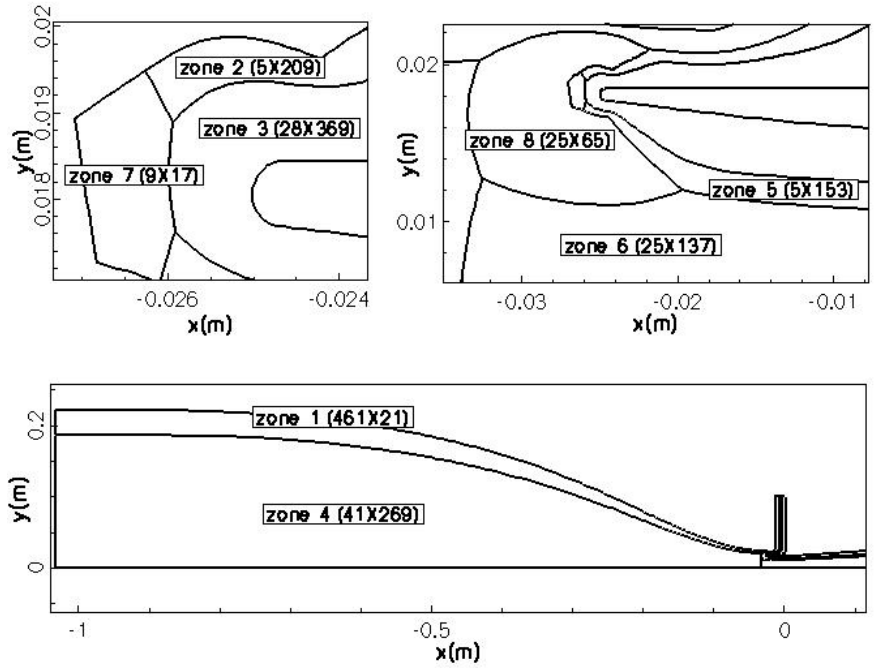

(a) Purdue Tunnel

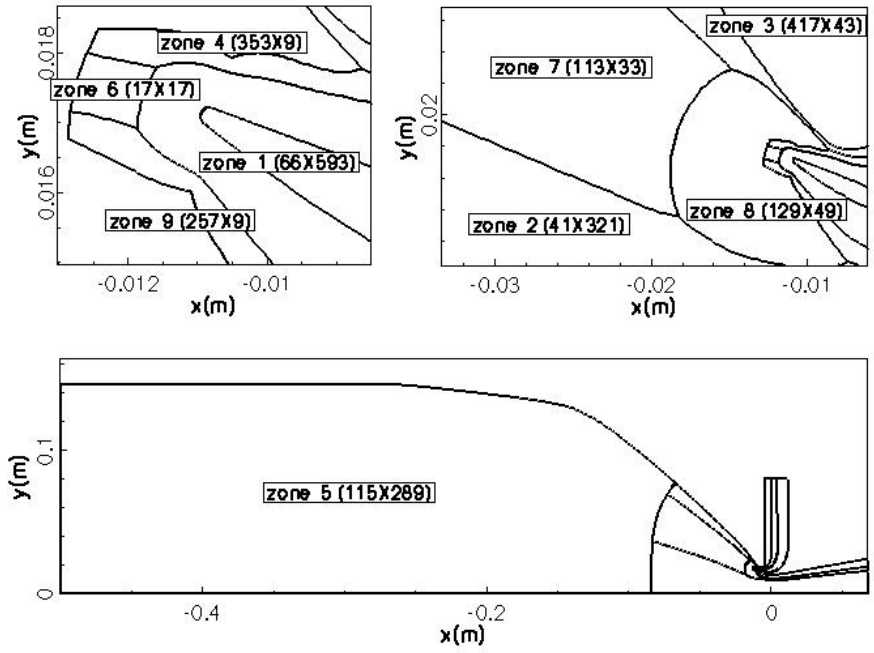

(b) Langley Tunnel

Figure 3. Zone Definitions

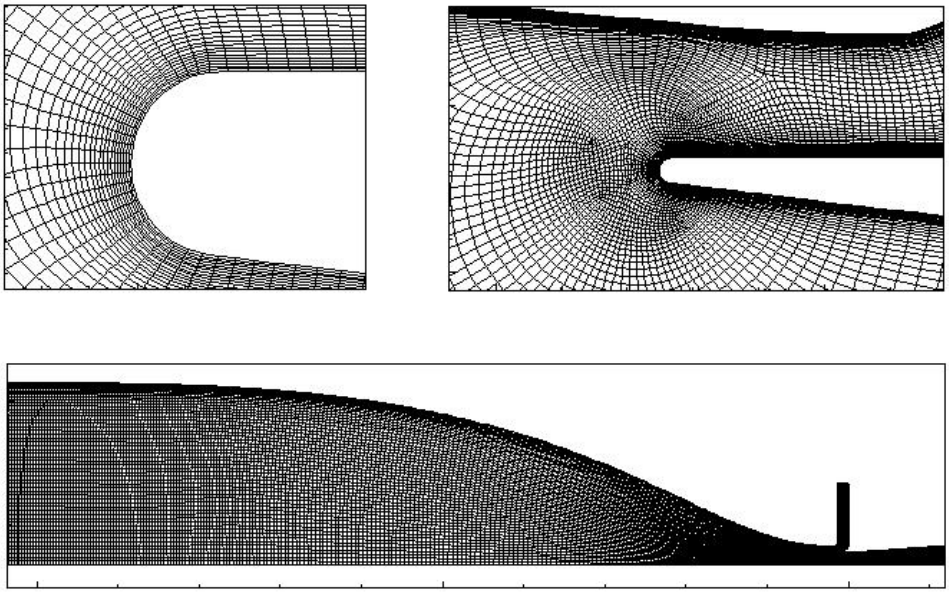

(a) Purdue Tunnel

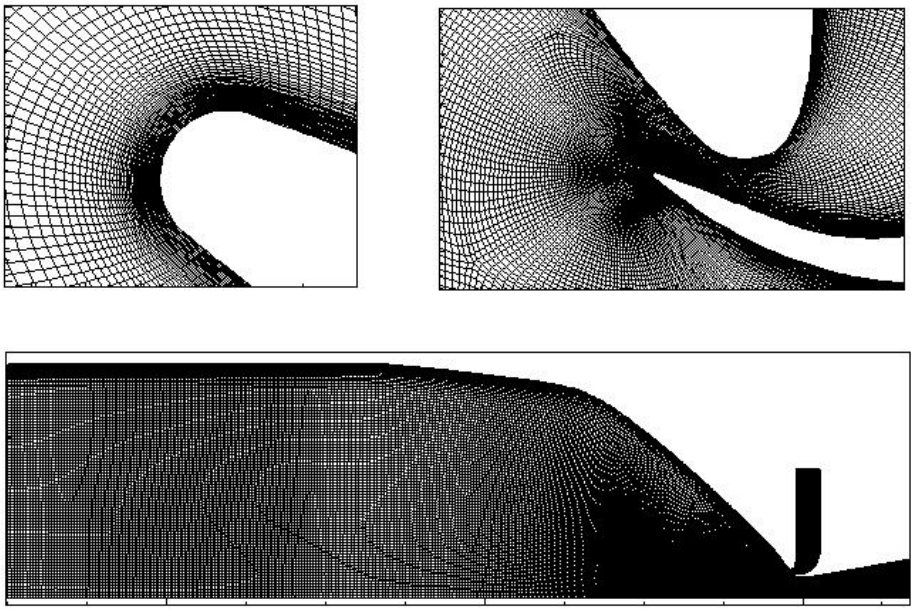

(b) Langley Tunnel

Figure 4. Grid

For run definitions, a steady state, laminar, axisymmetric flow solution is obtained for the flow conditions shown in Table 3.

Table 3. Flow conditions for the run definitions

Geometry	Purdue	Purdue	Langley	Purdue	Purdue
Flow Conditions	RUN1	RUN2	RUN3	RUN4	RUN5
$P_o(kPa)$	56	96.6	1034.2	56	96.6
$T_o(K)$	434	433	433	434	433
$\rho_o(kg/m^3)$	0.45	0.78	8.325	0.45	0.78
GRID	1	1	2	3	3

III. Numerical Algorithm

In this study a commercial flow solver, GASPex, Version 4.1.0+,[8] is used. GASPex solves the Reynolds-averaged compressible time-dependent Navier Stokes equations with a finite volume spatial discretization in which the state variables are stored at the cell centers. The accuracy of reconstructing the primitive variable field at the cell faces determines the spatial accuracy of the solution. The MUSCL approach is performed for variable extrapolation. In our computations, the inviscid flux scheme is chosen to be Roe's Method with the Harten entropy fix having third-order spatial accuracy reconstruction. The flux limiter is the Min Mod limiter. A steady state solution is obtained by applying the Gauss-Seidel relaxation scheme.

A. Boundary Conditions

For this axisymmetric flow domain, we have six physical boundaries two of which are symmetry wall surfaces where the "Negative (positive) axisymmetric wall boundary conditions" are applied. On the symmetry axis ($y = 0\ mm$) the "X-axis axisymmetric boundary condition" is implemented. For both of the outflow boundaries (bleed slot outlet and nozzle outlet at $x = 120\ mm$) the "Forced outflow" supersonic exit boundary condition is used. The existing inflow boundary conditions in GASPex, version 4.1.0+, did not work well since we have an extremely low incoming velocity in our problem. Therefore, a new subsonic inflow boundary condition was developed and added to the flow solver. The flow variables at the inflow boundary (denoted by subscript $_b$) for the new boundary condition are determined as follows:

1. Specify the inflow stagnation pressure P_{ob} and stagnation density ρ_{ob}
2. Assume positive axial velocity $u_b \geq 0$ with $M_b < 1$, and $v_b = w_b = 0$
3. Calculate the right running Riemann invariant R_c^- from:

$$R_c^- = u_c - \frac{2a_c}{\gamma - 1} \tag{1}$$

   where subscript $_c$ denotes the first interior cell.

4. Calculate the inflow Mach number M_b from:

$$\sqrt{\gamma \frac{P_{ob}}{\rho_{ob}}}(1 + \frac{(\gamma - 1)}{2} M_b^2)^{-\frac{1}{2}}(M_b - \frac{2}{\gamma - 1}) = R_c^- \tag{2}$$

5. Find the inflow pressure P_b from:

$$P_{ob} = P_b(1 + \frac{\gamma - 1}{2} M_b^2)^{\frac{\gamma}{\gamma - 1}} \tag{3}$$

6. Find the inflow density ρ_b from:

$$\rho_{ob} = \rho_b(1 + \frac{\gamma - 1}{2} M_b^2)^{\frac{1}{\gamma - 1}} \tag{4}$$

7. Calculate the inflow velocity u_b from:

$$u_b = M_b \sqrt{\gamma R T_b} \tag{5}$$

This boundary condition is called as "P_o-Riemann subsonic inflow" in GASPex, version 4.2.1 released in April 2004. The boundary conditions used in the analysis are tabulated in Table 4.

Table 4. Boundary conditions

Physical Boundary	Applied boundary condition
Solid wall	No slip, adiabatic
Slot exit	Forced outflow - supersonic exit
Nozzle exit	Forced outflow - supersonic exit
Inflow	New BC[a]
Side wall(s)	Negative (positive) axisymmetric wall
Symmetry	X-axis axisymmetric

IV. Results

In Fig. 5, the convergence history of the run definitions are shown. As it can be seen from this figure the residual level at convergence is larger for the higher stagnation inflow pressure for the Purdue tunnel (RUN2). The Purdue tunnel solutions are obtained with 40,000 iterations with a local CFL of 1. For the Langley tunnel simulation 30,000 iterations were performed with a local CFL of 1 (Figure 6). However, the bleed slot section was required to be extended further to be able to use the forced outflow boundary conditions correctly. The Langley tunnel results presented in this paper are the second run solutions with mesh sequencing obtained with the extended domain.

Inflow, exit and bleed slot exit mass flow rates obtained for each run definition are summarized in Table 5. For both run definitions of the Purdue tunnel 37% of the inflow mass leaves through the bleed slot. For the Langley tunnel, bleed slot mass flow is computed to be 25% of the inflow mass (Table 5). Mach number contours along with streamlines for the entire flow domain and for a close up view near the bleed slot are shown for RUN2 and RUN3 in Figure 6. Both the nozzle throat and the bleed slot throat are choked. The bleed slot geometry of Purdue tunnel has an elbow where flow is required to turn 90° yielding a recirculation region in the bleed slot on both walls. For the Langley tunnel, the flow has a smooth turn on the lower wall of the bleed slot elbow. Several shock structures are also seen in this region for both tunnels. The bleed slot is extended further to investigate the effect of the imposed outflow boundary condition at the slot exit for Purdue tunnel geometry. It is observed that the flow inside the nozzle displays the same flow behavior independent of the outflow boundary location for the slot.

In Fig. 7, streamtraces near the bleed slot are displayed for both run definitions RUN1 and RUN2 defined for the Purdue tunnel geometry. On the outer wall of the bleed slot lip, a recirculation region is observed

[a] P_o-Riemann subsonic inflow in GASPex, version 4.2.1

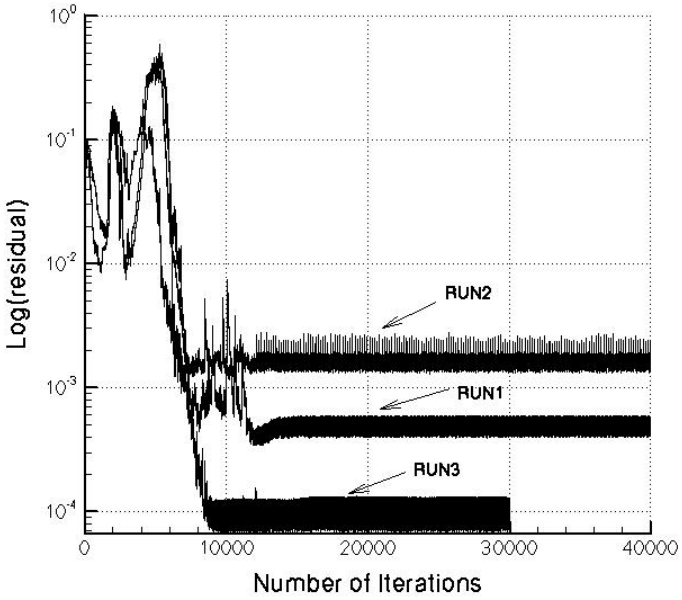

Figure 5. Convergence history for RUN1, RUN2 and RUN3

in both solutions. For RUN1, the flow solution recirculation length on the outer wall is 2.38mm. It is important to note that for this run definition, there is no reverse flow on the inner wall (Fig. 7a). For RUN2, the recirculation region on the outer wall is 2.66mm. In Fig. 7b, the nozzle wall below the slot is also zoomed in to detect any existing recirculation bubble. A very small recirculation zone (between points C and D in Fig. 7b) is seen. The recirculation length is 0.60 mm. In Fig. 8, streamtraces obtained for the Langley tunnel near the bleed slot lip are shown. At point A on the outer wall there is a very small reverse flow region of length 0.085mm (not seen in the figure), between points C and D on the inner wall a larger recirculation region of length 0.235mm is seen. Although grid resolution used for the Langley tunnel computations are comparable with the fine grid resolution used for the Purdue tunnel, a grid sensitivity analysis is necessary to quantify the error involved in the computations of the Langley tunnel.

A. Grid Sensitivity

Finer grid runs are performed for the Purdue tunnel in order to analyze the effect of the grid resolution on the numerical solution. The number of grid points for each zone and total number of grid points used in the grid sensitivity analysis are given in Table 6. The first cell height is reduced to 10^{-6} m. The results are given in Fig. 9. For an inflow stagnation pressure of 56 kPa, a recirculation bubble on the inner wall with length of approximately 0.37 mm is observed. For the same pressure RUN1 did not show this bubble. Given that the maximum height of recirculation region, approximately 0.005 mm, is smaller than the first cell height used for RUN1 (10^{-5} m), it is clear why this bubble was not seen in the solutions of RUN1. On the outer wall the reverse flow region length is computed to be 2.61 mm. For an inflow stagnation pressure of 96.6 kPa, similar to the solution of RUN2, a recirculation bubble on the nozzle wall with maximum height of approximately 0.018 mm is seen. The recirculation region length on the inner and outer wall is approximately 0.71, and 3.06 mm, respectively. A summary of the computed recirculation lengths can be seen in Table 7.

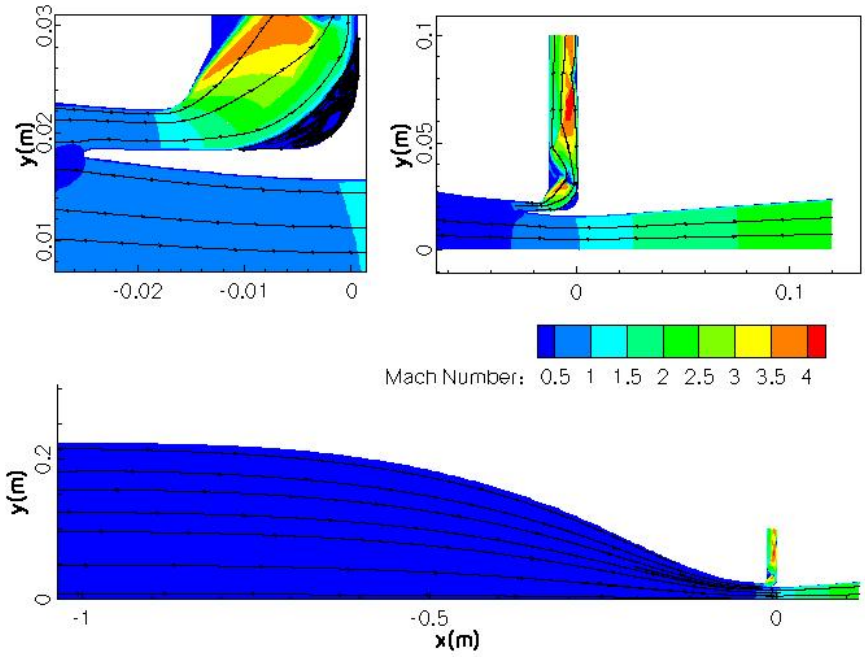

(a) Purdue Tunnel (RUN2 $P_o = 96.6kPa$)

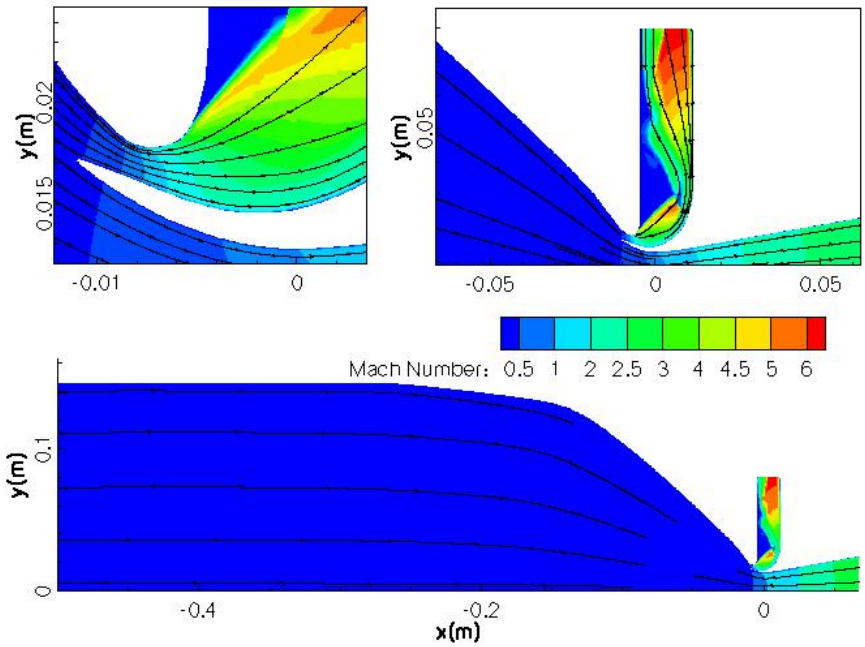

(b) Langley Tunnel (RUN3 $P_o = 1034.2kPa$)

Figure 6. Mach Contours and Streamtraces

Table 5. Inflow and outflow mass flow rates for run definitions

RUN1	Mass flow rate(g/s)
Inflow	132.8
Outflow	82.4
Bleed Slot	49.6
RUN2	
Inflow	228.8
Outflow	142.4
Bleed Slot	85.6
RUN3	
Inflow	1339.2
Outflow	1003.2
Bleed Slot	336.3
RUN4	
Inflow	132.4
Outflow	82.6
Bleed Slot	49.7
RUN5	
Inflow	229.7
Outflow	143.1
Bleed Slot	86.5

Table 6. Grid size of each zone for grid sensitivity analysis for Grid No.3 - Purdue Tunnel

Zone	1	2	3	4	5	6	7	8
Grid	777×76	257×17	60×545	129×537	273×17	81×257	17×49	113×33
							Total	$= 195,414$

V. Conclusions and Future Studies

The main conclusions of this study are as follows:

- For the Purdue tunnel, our results show that as the inflow stagnation pressure increases the recirculation bubble formed on the nozzle wall becomes bigger. This suggest an explanation for having quiet tunnel performances only for low stagnation pressures of 8 *psia* for bleed slot design case 7.[5]
- Although the Langley tunnel computations displayed reverse flow regions on both walls of the bleed slot tip, the recirculation length is smaller than that seen in the Purdue tunnel computations. This might be due to the position and shape of the bleed slot lip or/and the contour of the contraction wall, but the size of the bleed slot lip must also be taken into account. It is important to note that the bleed slot tip diameter is three times smaller for the Langley tunnel.
- Although flow in the bleed slot is choked, and noise should not travel upstream, it still seems preferable to redesign the bleed-slot elbow section to eliminate the separation bubble. It appears simplest to do

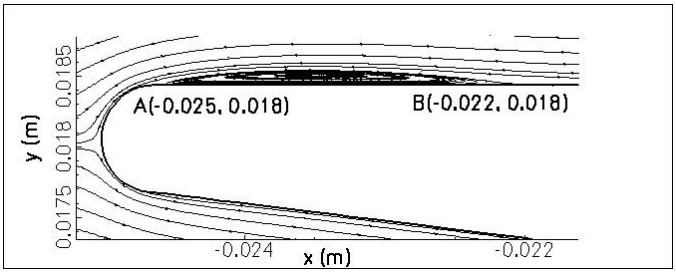

(a) at $P_o = 56\ kPa$

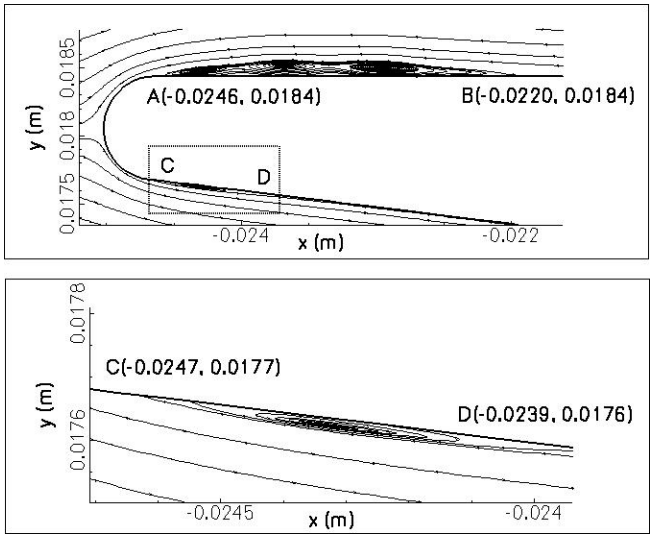

(b) at $P_o = 96.6\ kPa$

Figure 7. Streamtraces for the Purdue Tunnel with Grid No.1

so by fairing a larger-radius curve into the corner.

The next step of this study is to conduct an automated design optimization to minimize the recirculation length observed on the walls of the bleed slot lip.

VI. Acknowledgement

The authors would like to thank to Mr. Shin Matsumura for the preparation of the geometry data required for the numerical analysis of the Langley tunnel.

References

[1]Bertin, J. J. and Cummings, R. M., "Fifty Years of Hypersonics: Where We've Been, Where We're Going," *Progress in Aerospace Sciences*, Vol. 39, 2003, pp. 511–536.

[2]Schneider, S. P., "Effects of High Speed Tunnel Noise on Laminar-Turbulent Transition," *J Spacecraft Rockets*, Vol. 38,

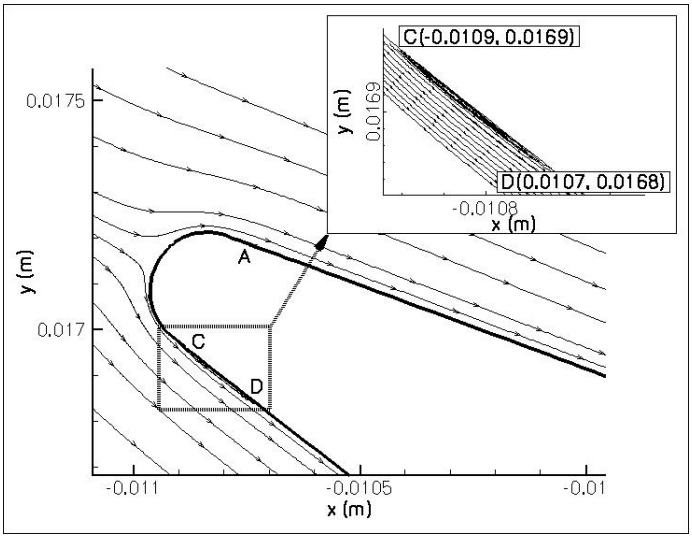

Figure 8. Streamtraces for the Langley Tunnel at $P_o = 1034.214\ kPa$

Table 7. Summary of computed recirculation lengths in mm*

	Inner wall	Outer wall
RUN1	0.00	2.38
RUN2	0.60	2.66
RUN3	0.235	0.085
RUN4	0.37	2.61
RUN5	0.71	3.06

*the length is calculated based on velocity sign change

No. 3, 2001, pp. 323–33.

[3]Schneider, S. P., , Skoch, C., Rufer, S., Matsumura, S., and Swanson, E., "Transition Research in the Boeing/AFOSR MACH-6 Quiet Tunnel," *AIAA Paper 2002-0302*, Jan. 2002.

[4]Schneider, S. P. and Skoch, C., "Progress in the Operation of the Boeing/AFOSR Mach-6 Quiet Tunnel," *AIAA Paper 2002-3033*, June 2002.

[5]Schneider, S. P., Matsumura, S., Rufer, S., Skoch, C., and Swanson, E., "Hypersonic Transition Research in the Boeing/AFOSR Mach-6 Quiet Tunnel," *AIAA Paper 2003-1130*, Jan. 2003.

[6]Benay, R., Chanetz, B., Coponet, D., Thobis, P., and Seraudie, A., "Tache 1 du PRF Etudes D'ecoulements Relatifs a L'avion Supersonique: Travaux Realises an 2002," Rapport Technique RT 9/06671 DMAE/DAE, ONERA, France, In French, Translated at Purdue University, March 2003.

[7]Benay, R., Chanetz, B., and Gherardi, B., "Design of a Boundary Layer Suction Device for a Supersonic Quiet Wind Tunnel by Numerical Simulation," *Aerospace Science and Technology*, Vol. 8, 2004, pp. 255–271.

[8]Aerosoft Inc., Blacksburg, VA, *General Aerodynamic Simulation Program User Manual*, 1996.

[9]Program Development Corporation, White Plains, New York, *GridPro/az3000 User's Guide and Reference Manual*, 1998.

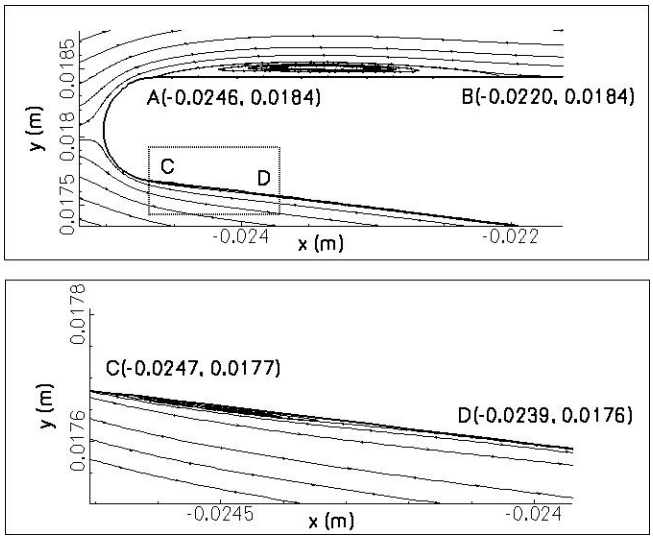

(a) at $P_o = 56\ kPa$

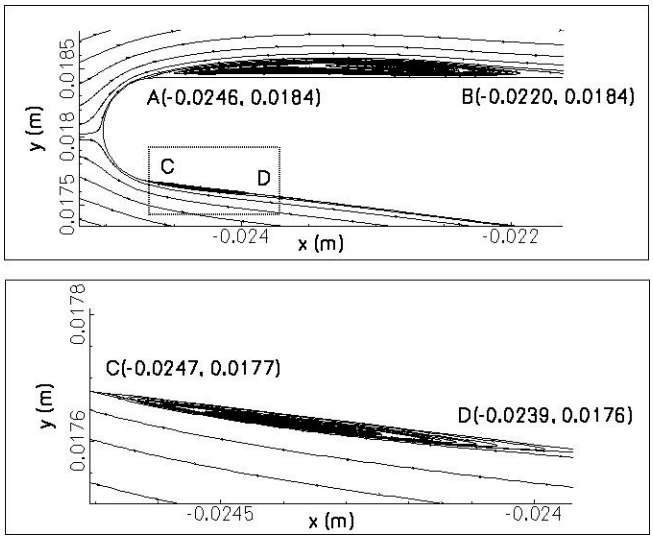

(b) at $P_o = 96.6\ kPa$

Figure 9. Streamtraces for the Purdue Tunnel with Grid No.3